Journal of Animal & Plant Sciences, 35(6): 2025, Page: 1679-1690
ISSN (print): 1018-7081; ISSN (online): 2309-8694
https://doi.org/10.36899/JAPS.2025.6.0141

EFFECT OF SHIKONIN ON THE UTERINE PATHOLOGICAL CHANGES IN UTERINE MYOMA MICE BY SUPPRESSING THE ACTIVATION OF MAPK/ERK PATHWAY

J. H. Wang

Department of Obstetrics and Gynecology, Changsha Hospital of Hunan Normal University, The Fourth Hospital of Changsha, Changsha, 410000, Hunan, China.
Corresponding Author Email: wangjianhua608@126.com

ABSTRACT

Uterine myoma (UM) is a benign tumor primarily characterized by clonal proliferation of uterine smooth muscle (USM) cells, with contributions from genetic and hormonal factors, and exhibits a high incidence rate. Shikonin (SHK), a bioactive naphthoquinone derived from Lithospermum erythrorhizon, exhibits potent anti-inflammatory and antitumor properties. This work investigated the effects of SHK on the uterine pathological conditions in UM mice and analyzed its potential mechanism of anti-UM activity based on the Mitogen-Activated Protein Kinase/Extracellular Signal-Regulated Kinase (MAPK/ERK) pathway. Thirty-six female ICR mice were randomly divided into six groups: Blank control group (BC group), UM model group (UM group), Positive control group (PC group), Low-dose SHK group (Low-SHK group), Middle-dose SHK group (Middle-SHK group), and High-dose SHK group (High-SHK group), with six mice in each group. The UM model was induced by intramuscular injection of estradiol benzoate for 15 consecutive days, and the validity of the model was confirmed through uterine tissue histopathology (thickening of the smooth muscle layer and infiltration of inflammatory cells) and serum hormone levels (significant elevation of estradiol and progesterone)), Positive control group (PC group; continuous gavage of 0.1 μg/g estradiol valerate after modeling, Low-dose SHK group (Low-SHK group; continuous gavage of 100 μg/g SHK after modeling), Middle-dose SHK group (Middle-SHK group; continuous gavage of 200 μg/g SHK after modeling) and High-dose SHK group (High-SHK group; continuous gavage of 400 μg/g SHK after modeling), with six mice in each. Blood was collected from the heart to detect serum sex hormone levels, and the uterus was taken after death. Hematoxylin-eosin staining was used to observe the pathological changes in the tissue. Real-time fluorescent quantitative PCR and Western blotting were adopted to detect the distinctions in the expression of apoptosis-related mRNA [Bax, Bcl-2, and Caspase-3 (Cas-3)] and MAPK/ERK pathway-related proteins (p38 MAPK and ERK) in the uterus. As against BC group, in UM group, the weight of the uterus, the vertical/horizontal diameter, the organ coefficient, and the thickness of the smooth muscle all increased; the arrangement of USM cells was disordered, and there was inflammatory cell infiltration; the levels of serum estradiol, progesterone, luteinizing hormone, estrogen receptor, progesterone receptor, and follicle-stimulating hormone all increased, while the level of anti-Müllerian hormone (AMH) decreased; the expression of Bax and Cas-3 in the uterus decreased, while the expression of Bcl-2 increased; the phosphorylation levels of p38 MAPK and ERK in the uterus increased ($P \leq 0.05$). As against UM group, in PC group, Low-SHK group, Middle-SHK group and High-SHK group, the weight of the uterus, the vertical/horizontal diameter, the organ coefficient, and the thickness of the smooth muscle all decreased; the pathological changes in the uterus were alleviated; serum estradiol, progesterone, luteinizing hormone, estrogen receptor, progesterone receptor, and follicle-stimulating hormone all decreased, while AMH increased; the expression of Bax and Cas-3 in the uterus increased, while the expression of Bcl-2 decreased; the phosphorylation levels of p38 MAPK and ERK in the uterus decreased ($P \leq 0.05$). With the increase of SHK dosage, the changes in the morphology of the uterus, the histopathological morphology, the serum sex hormones, the expression of apoptosis-related mRNA in the uterus, and the expression of MAPK/ERK pathway-related proteins became more obvious ($P \leq 0.05$). SHK suppressed UM progression by reducing uterine weight, vertical/horizontal diameters, and smooth muscle thickness, while restoring serum sex hormone balance and promoting apoptosis via Bax/Cas-3 upregulation and Bcl-2 downregulation. These effects were mediated through dose-dependent inhibition of MAPK/ERK pathway activation.

Keywords: Uterine myoma; Shikonin; uterine morphology; sex hormones; apoptosis; MAPK/ERK pathway.

Published first online October 08, 2025 Published final November 30, 2025

INTRODUCTION

Uterine myoma (UM) has an incidence rate of about 20-25% in women of childbearing age. They are characterized by multiplicity and recurrence, and have seriously affected women's fertility (Donnez *et al*., 2024). Moreover, studies have confirmed that UM also have the risk of malignancy (Fasciani *et al*., 2023). The etiology of UM involves complex interactions between sex hormones and signaling pathways such as MAPK/ERK, which regulates cell proliferation and apoptosis. Dysregulation of MAPK/ERK signalling has been implicated in UM pathogenesis (Shafiee *et al.,* 2017; Afrin *et al.,* 2023). While sex hormones are central to UM progression, genetic mutations (*e.g.,* MED12) and aberrant pathway activation further drive tumor growth. Exogenous administration of estrogen in combination with P can induce the construction of animal models of UM (Ahmad *et al*., 2023). Clinically, UM is mainly treated by surgical resection or drug control. Since uterine body fibroid accounts for 90% of all UM, the recurrence rate after surgical resection is high (Lee and Stewart, 2023).

Given the limitations of current therapies, natural compounds with multi-target regulatory effects have gained attention as potential alternatives for UM treatment. Lithospermum has the outcomes of cooling blood, activating blood circulation, and detoxifying (Barkizatova *et al*., 2024). Shikonin (SHK) is a purple-red compound extracted from the roots of plants in certain genera (such as Lithospermum or Arnebia), and has been widely investigated for its antitumor activity. It induces apoptosis in cervical cancer cells by downregulating key glycolytic enzymes through signalling pathways such as PI3K/AKT/HIF-1α and JAK2/STAT3 (Liu *et al.,* 2024). SHK derivative PMMB232 exhibits a dose-dependent effect in inhibiting the proliferation of cervical cancer Hela cells (Han *et al.,* 2018). These studies provide a theoretical foundation for the application of SHK in UM treatment (Sun *et al*., 2022; Yadav *et al*., 2022). Moreover, SHK has anti-tumor activity in multiple cancers. It plays a role in cancer treatment (Yan *et al*., 2023). SHK can suppress the growth of small cell lung cancer xenografts (Qian *et al*., 2023). Nanoparticle drug delivery systems loaded with SHK can be combined with tumor-related CD44 to achieve targeted delivery of colorectal cancer, and inhibit the proliferation and migration of tumor cells by reversing the epithelial-mesenchymal transition (Long *et al*., 2023). SHK in combination with cisplatin can reduce the survival rate of cisplatin-resistant ovarian cancer cells and also inhibit the growth of tumors in BALB/c nude mice xenografts (Ni *et al*., 2023). SHK exhibits a variety of anti-tumor activities, but its potential mechanism in treating UM remains to be further explored.

Despite SHK's established antitumor effects, its specific mechanisms in UM, particularly its interaction with the MAPK/ERK pathway and sex hormone regulation, have not been systematically investigated. This study aims to address this gap by evaluating the dose-dependent effects of SHK on UM pathology and MAPK/ERK signaling in a hormone-induced mouse model.

MATERIALS AND METHODS

Animals: Thirty-six clean-grade female ICR mice (18-22 g; Liaoning Changsheng Biotechnology Co., Ltd., China) were adopted as the subjects of the work. All mice were housed in the clean-grade animal experimental room of the Experimental Animal Center, with a room temperature of 20-25℃, relative humidity of 50-60%, and a 12 h/12 h light-dark cycle, and were allowed free access to food and water. The experimental procedures involved obtained the approval by the Animal Care and Use Committee of The Fourth Hospital of Changsha. All animal housing and experiments were strictly conducted based on the institutional guidelines. ICR mice were selected for the experiment due to their high sensitivity to hormone-induced uterine fibroid models and their reproductive system structure, which closely resembles that of humans. These mice have been widely used in UM research (Lee and Stewart, 2023; Yousefi *et al.,* 2021).

Grouping and treatment: The mice were randomly divided into: Blank control group (BC group), UM model group (UM group), Positive control group (PC group), Low-dose SHK group (Low-SHK group), Middle-dose SHK group (Middle-SHK group) and High-dose SHK group (High-SHK group), with six mice in each group. The SHK doses (100, 200, and 400 μg/g) were determined based on preliminary experimental results: the low dose (100 μg/g) was close to the half-maximal effective concentration (EC50), while the medium and high doses were increased by 2-fold and 4-fold, respectively, to assess dose-dependent effects (Sun *et al.,* 2022).

BC group: Intramuscular injection of 0.9% sodium chloride at 0.1 mL/10 g. UM group: A mixture of 2 mL estradiol benzoate (Shanghai Macklin Biochemical Co., Ltd., China), 2 mL Tween80 (Beyotime Institute of Biotechnology, China), and 96 mL 0.9% sodium chloride was prepared. Intramuscular injection of the estradiol benzoate mixture at 0.1 mL/10 g, daily, for 15 d. Uterine uterine myoma were induced by continuous intramuscular injection of a mixed solution consisting of estradiol benzoate (2 mL), Tween 80 concentration was 2% v/v (2 mL), and 0.9% saline (96 mL) at a dosage of 0.1 mL/10 g for 15 consecutive days. This method has

been successfully validated in mouse models (Mamoon *et al.,* 2021; Yousefi *et al.,* 2021).

PC group: Intramuscular injection of the estradiol benzoate mixture at 0.1 mL/10 g, daily, for 15 d. After successful modeling, gavage treatment with 0.1 μg/g estradiol valerate tablets (Bayer Healthcare Co., Ltd., Guangzhou Branch, China) was administered, daily, for 15 d. Following model establishment, the mice were continuously gavaged with 0.1 μg/g estradiol valerate tablets (Bayer). Estradiol valerate, a commonly used clinical hormonal regulator, can reduce fibroid volume by antagonizing estrogen receptors and has been used as a positive control in UM treatment studies (Ali *et al.*, 2022; Beck *et al.,* 2022).

Low-SHK group: Intramuscular injection of the estradiol benzoate mixture at 0.1 mL/10 g, daily, for 15 d. After successful modeling, gavage treatment with 100 μg/g low-dose SHK (Sichuan Jingcuibao Biotechnology, China) was administered, daily, for 15 d.

Middle-SHK group: Intramuscular injection of the estradiol benzoate mixture at 0.1 mL/10 g, daily, for 15 d. After successful modeling, gavage treatment with 200 μg/g middle-dose SHK was administered, daily, for 15 d.

High-SHK group: Intramuscular injection of the estradiol benzoate mixture at 0.1 mL/10 g, daily, for 15 d. After successful modeling, gavage treatment with 400 μg/g high-dose SHK was administered, daily, for 15 d.

Uterine morphological examination: After the end of drug administration, mice were subjected to anesthesia by 0.3% pentobarbital sodium (Sigma-Aldrich, USA) at 50 mg/kg. Blood was collected from the heart, and then the mice were euthanized by cervical dislocation. The abdominal cavity of the mice was routinely opened to observe the morphological changes of the uterus. The uterus was separated and weighed, and the maximum transverse and vertical diameters were measured with a vernier caliper. The uterine coefficient was calculated according to the equation (uterine weight/body weight×100%).

Hematoxylin-eosin staining: The mouse uterine tissues were immersed in 4% paraformaldehyde (Sigma-Aldrich, USA) for fixation for 1 day, routinely embedded in paraffin and continuously sectioned to make paraffin sections with a thickness of 4 μm. The uterus paraffin sections were stained with a hematoxylin-eosin staining kit (Beyotime Biotechnology, China), and the pathological morphological changes of the uterine tissue were observed under an optical microscope. Pathological scoring was also conducted. Some uterine tissues were fixed in 4% paraformaldehyde (Sigma-Aldrich, USA) for 24 hours. After dehydration through a graded ethanol series and clearing in xylene, the tissues were embedded in paraffin and sectioned continuously at a thickness of 4 μm. The sections were deparaffinized, hydrated, and stained with hematoxylin (Beyotime Biotechnology, China) for 5 minutes, followed by rinsing in running water to blue. Subsequently, they were stained with eosin (Beyotime Biotechnology, China) for 2 minutes, dehydrated through a graded ethanol series, cleared in xylene, and mounted with neutral gum (Solarbio, China). Stained sections were observed and photographed using a Nikon optical microscope (Nikon ECLIPSE Ci-L, Japan) at ×100 and ×400 magnification. Pathological scoring was performed by two independent researchers using a blinded method to eliminate subjective bias.

The scoring criteria were as follows: (1) Inflammatory cell infiltration. No inflammatory cell infiltration was scored as 0; a small amount of inflammatory cell infiltration was scored as 1; a small amount of inflammatory cell infiltration in the mucosal lamina propria, or inflammatory cell infiltration in foci or extending to the muscular layer was scored as 2; inflammatory cell infiltration in layers and involving the whole layer was scored as 3. (2) Thickness of the uterine wall smooth muscle. No obvious change in the thickness of the uterine wall smooth muscle was scored as 0; mild diffuse hyperplasia of the uterine wall smooth muscle was scored as 1; local thickening of the uterine wall smooth muscle, leading to uneven thickness of the muscular layer was scored as 2; multiple thickening of the uterine wall smooth muscle, leading to high unevenness of the uterine wall, or hyperplasia extending to the mesometrium was scored as 3.

ELISA: Blood was collected from the heart and centrifuged at 3,000 rpm/min for 15 min at 4℃. After the serum was separated, the levels of serum estradiol, progesterone, luteinizing hormone, estrogen receptor, progesterone receptor, follicle-stimulating hormone, AMH in the serum were detected using an ELISA (Beyotime Biotechnology, China).

Real-time fluorescent quantitative PCR experiment: Partial uterine tissues were taken and total RNA was extracted by adding Trizol reagent (Sigma-Aldrich, USA). The first-strand cDNA was synthesized using a reverse transcription kit (Takara Biomedical Technology (Beijing) Co., Ltd., China), and then the target genes were amplified using a real-time fluorescent quantitative PCR kit (Takara Biomedical Technology (Beijing) Co., Ltd., China) with the synthesized cDNA as the template. GAPDH was adopted as the internal reference gene, and the relative expression of Bax, Bcl-2, and Cas-3 were calculated according to the $2^{-\triangle\triangle CT}$ method. The primer information for Bax quantification was: upstream 5'-CCGGCGAATTGGAGATGAACT-3', downstream 5'-CCAGCCCATGATGGTTCTGAT-3'; Bcl-2: upstream 5'-GTCGCTACCGTCGTGACTTC-3', downstream 5'-CAGACATGCACCTACCCAGC-3'; Cas-3: upstream 5'-CTGACTGGAAAGCCGAAACTC-3', downstream 5'-CGACCCGTCCTTTGAATTTCT-3'; GAPDH:

upstream 5'-TGGCCTTCCGTGTTCCTAC-3', downstream 5'-GAGTTGCTGTTGAAGTCGCA-3'.

Western blotting: Partial uterine tissues were taken, homogenized with RIPA reagent (Sigma-Aldrich, USA), and then total proteins were extracted. The concentration of the proteins was detected adopting a BCA quantification detection kit (Thermo Fisher Scientific, USA). After adding loading buffer (5×), the proteins were boiled at 100℃ for 5 min to denature, and then subjected to separating. Transfer onto a PVDF membrane was carried out, blocking with 5% skimmed milk powder (Beyotime Biotechnology, China) at 25℃ for 1 h. After washing, first antibodies (Ab) against p38 MAPK, p-p38 MAPK, ERK, p-ERK, and β-actin (diluted at a ratio of 1:1000; Abcam, UK) were applied. incubation overnight at 4℃. β-Actin served as the loading control to ensure equal protein loading across samples. Band intensities were normalized to β-actin for quantitative analysis. After washing again, horseradish peroxidase-conjugated goat anti-rabbit IgG secondary Ab (diluted at a ratio of 1:5000, Abcam company, UK) was applied, incubation at 25℃ for 2 h. After washing, the proteins were visualized using an enhanced chemiluminescence substrate kit (Thermo Fisher Scientific, USA), and the relative gray values of protein expression were analyzed using ImageJ software.

Statistical methods: All data were expressed as mean ± standard deviation ($\bar{x}\pm s$) and were statistically analyzed using *SPSS 23.0* and *GraphPad Prism 9.0*. One-way ANOVA was adopted and independent sample *t*-test was adopted for contrast. *P* value of less than 0.05 was considered statistically significant.

RESULTS

Effects on uterine morphology: Figure 1A shows the comparison of uterine tumor volumes in different groups of mice. The average uterine tumor volume in the UM group was 1.25 ± 0.18 cm^3, significantly higher than that in the BC group (0.15 ± 0.03 cm^3, $P \leq 0.001$). The High-SHK group exhibited a volume reduction to 0.42 ± 0.07 cm^3 (*vs.* UM group, $P \leq 0.001$), a decrease of 66.4%. The Middle- and Low-SHK groups showed reductions of 49.6% and 28.8%, respectively (Figure 1A). Figure 1B presents the vertical diameter measurement results of the uterus. The average vertical diameter in the UM group was 10.3 ± 1.5 mm, significantly higher than that in the BC group (2.8 ± 0.4 mm, $P \leq 0.001$). The High-SHK group showed a reduction in diameter to 3.9 ± 0.6 mm (*vs.* UM group, $P \leq 0.001$), a decrease of 62.1%. The Middle- and Low-SHK groups showed reductions of 44.7% and 21.4%, respectively (Figure 1C). Figure 1C shows the horizontal diameter measurement results of the uterus. The average horizontal diameter in the UM group was 10.3 ± 1.5 mm, significantly higher than that in the BC group (2.8 ± 0.4 mm, $P \leq 0.001$). The High-SHK group showed a reduction in diameter to 3.9 ± 0.6 mm (*vs.* UM group, $P \leq 0.001$), a decrease of 62.1%. The Middle- and Low-SHK groups exhibited reductions of 44.7% and 21.4%, respectively (Figure 1C). Figure 1D shows the uterine coefficient. The average uterine coefficient in the UM group was 0.85 ± 0.12, significantly higher than that in the BC group (0.10 ± 0.02, $P \leq 0.001$). The high-dose SHK group exhibited a reduction in the coefficient to 0.28 ± 0.05 (*vs.* UM group, $P \leq 0.001$), a decrease of 67.1%. The Middle- and Low-SHK groups showed reductions of 52.9% and 30.6%, respectively (Figure 1D). Figure 1E presents the thickness of the USM layer (μm). The average smooth muscle layer thickness in the UM group was 250 ± 35 μm, significantly higher than that in the BC group (50 ± 8 μm, $P \leq 0.001$). The High-SHK group showed a reduction in thickness to 90 ± 15 μm (*vs.* UM group, $P \leq 0.001$), a decrease of 64.0%. The Middle- and Low-SHK groups exhibited reductions of 48.0% and 28.0%, respectively (Figure 1E).

Effects of uterine tissue pathology: In Figure 2A, HE staining shows that in the BC group, USM cells were arranged neatly with regular morphology, and no significant inflammation or hyperplasia was observed. In the UM group, USM cell arrangement was disorganized, with focal necrosis in local areas (indicated by arrows), and the smooth muscle layer was significantly thickened (average thickness: 2.5 μm *vs.* BC group 0.2 μm, $P \leq 0.05$), accompanied by extensive infiltration of lymphocytes and neutrophils (Figure 2B, score 3). In the SHK treatment group (using the high-dose group as an example), USM cell arrangement became more regular, with reduced necrotic areas (Figure 2A, dashed box). The smooth muscle thickness decreased to 1.3 μm (*vs.* UM group, $P \leq 0.05$), and the inflammatory cell infiltration score decreased to 1 (Figure 2B). In Figure 2B to 2C, the scores for inflammatory cell infiltration and the thickness of the uterine wall smooth muscle in the UM group were markedly higher in contrast to BC group; the scores for inflammatory cell infiltration and the thickness of the uterine wall smooth muscle in PC group, Low-SHK group, Middle-SHK group and High-SHK group were markedly lower in contrast to UM group; with the increase of SHK dosage, the scores for inflammatory cell infiltration and the thickness of the uterine wall smooth muscle in Low-SHK group, Middle-SHK group and High-SHK group gradually decreased ($P \leq 0.05$).

Effects of sex hormone levels: In Figure 3A to 3G, the levels of peripheral blood serum estradiol (Figure 3A), progesterone (Figure 3B), luteinizing hormone (Figure 3C), estrogen receptor (Figure 3D), progesterone receptor (Figure 3E), and follicle-stimulating hormone (Figure 3F)

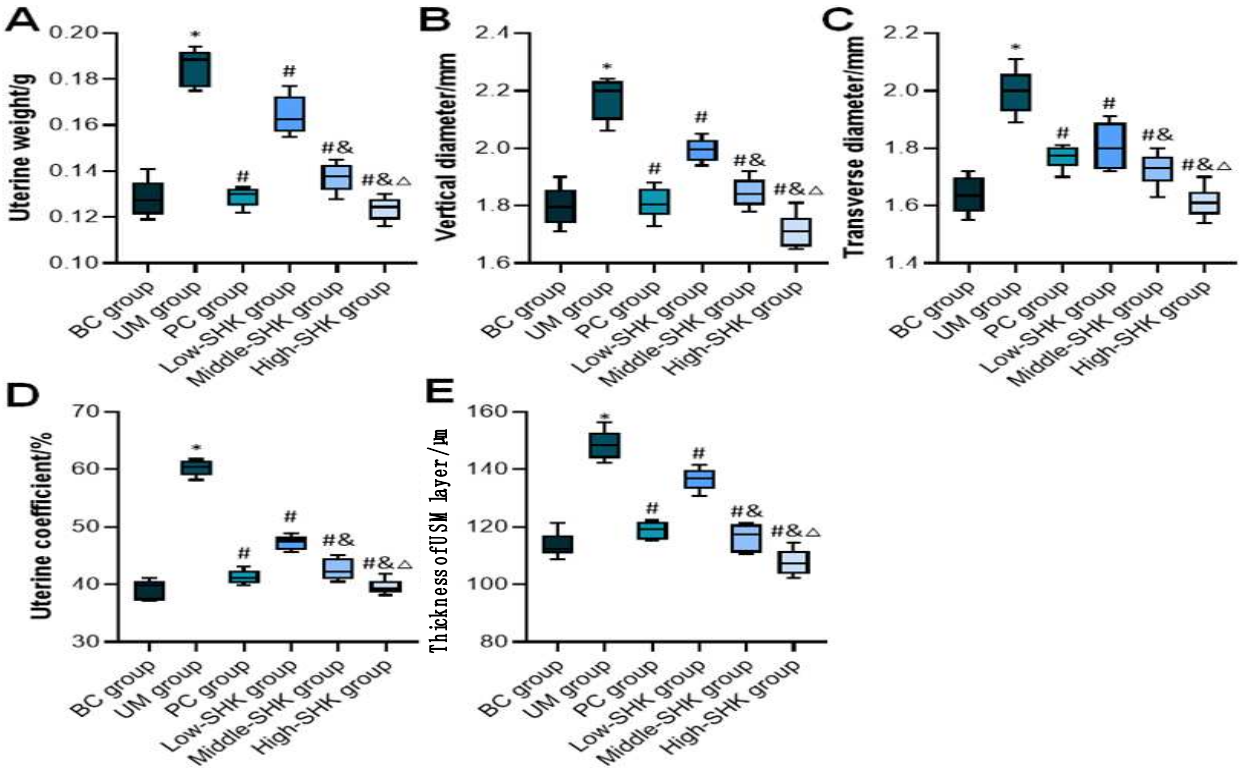

Fig. 1 Comparison of distinctions in uterine morphological parameters of mice. A: uterine tumors volumes; B: vertical diameter of the uterus; C: horizontal diameter of the uterus; D: uterine coefficient; E: thickness of USM. * Compared with BC group, $P \leq 0.05$; # compared with UM group, $P \leq 0.05$; & compared with Low-SHK group, $P \leq 0.05$; △ compared with Middle-SHK group, $P \leq 0.05$.

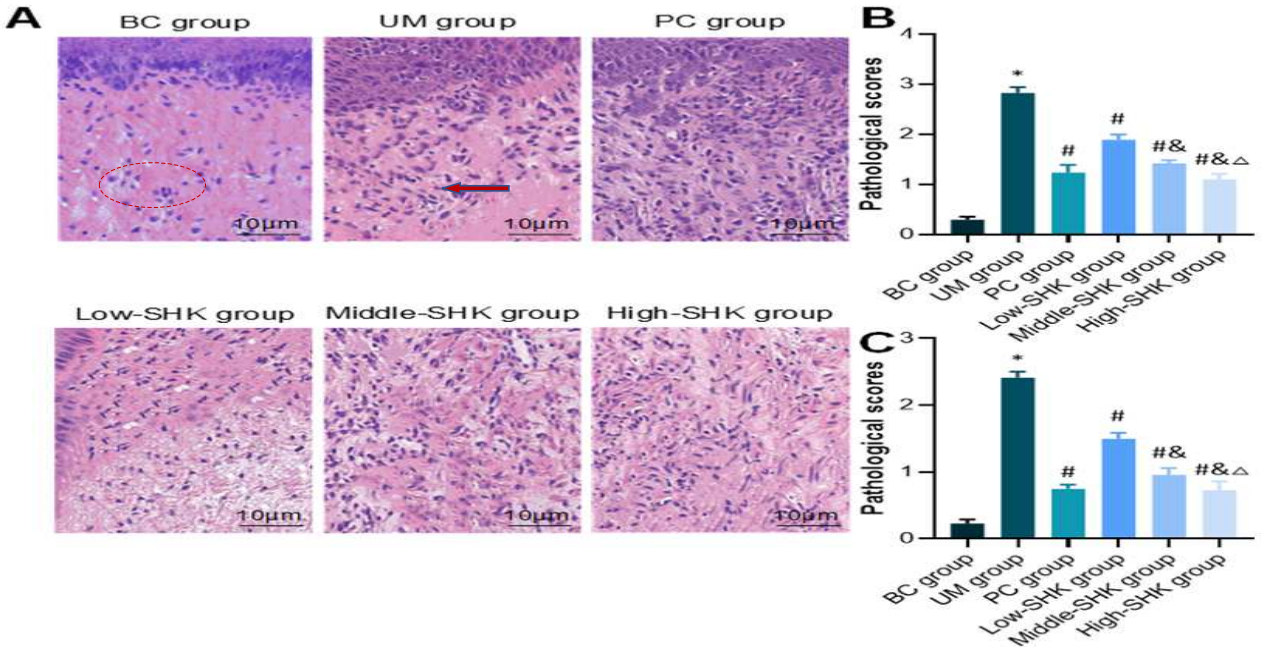

Fig. 2 Comparison of distinctions in uterine tissue pathology of mice. A: observation of uterine HE staining (×100); B: score of inflammatory cell infiltration; C: score of the thickness of the uterine wall smooth muscle. * Compared with BC group, $P \leq 0.05$; # compared with UM group, $P \leq 0.05$; & compared with Low-SHK group, $P \leq 0.05$; △ compared with Middle-SHK group, $P \leq 0.05$.

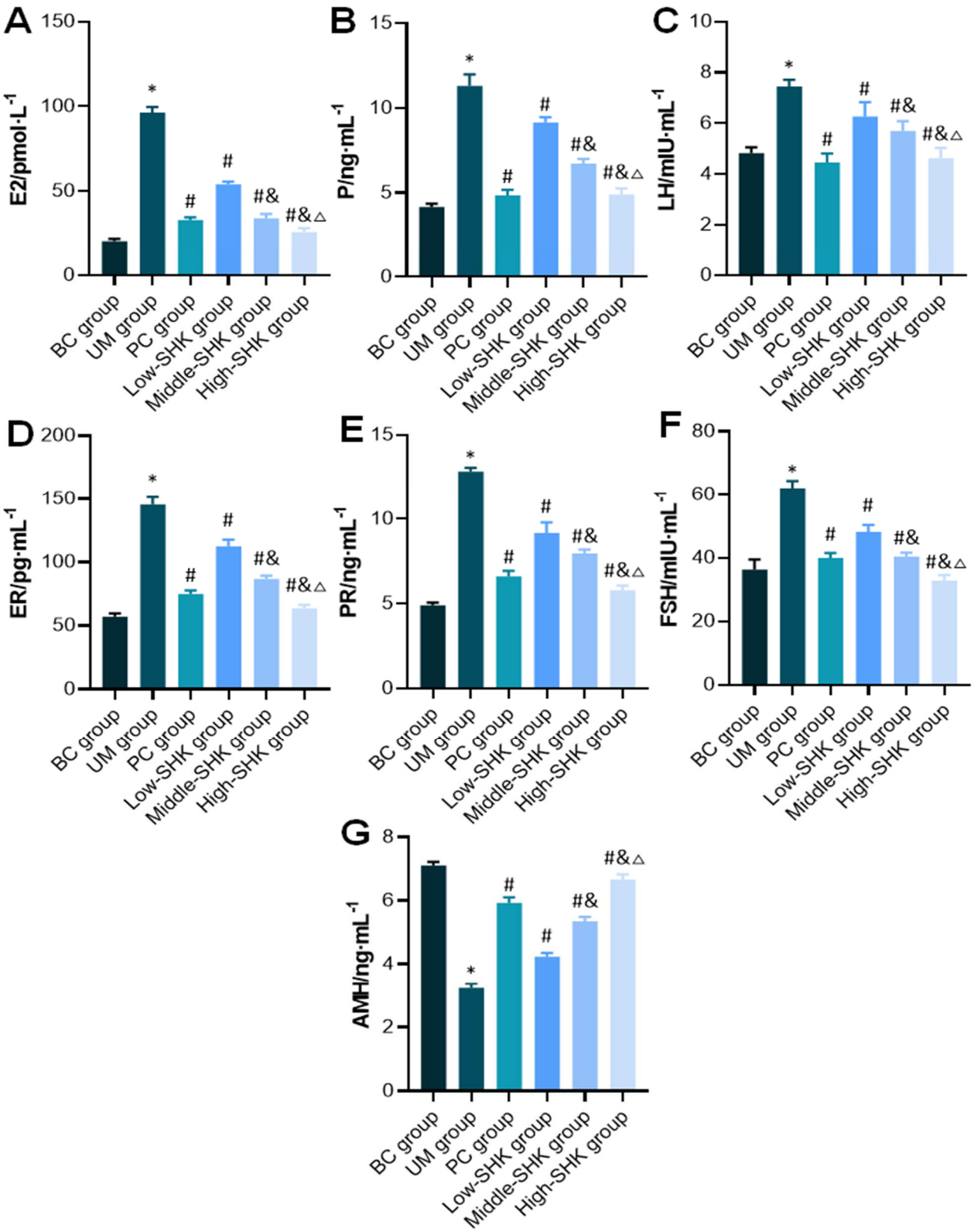

Fig. 3 Comparison of distinctions in sex hormone levels of mice. A: serum estradiol; B: progesterone; C: luteinizing hormone; D: estrogen receptor; E: progesterone receptor; F: follicle-stimulating hormone; G: AMH. * Compared with BC group, $P \leq 0.05$; # compared with UM group, $P \leq 0.05$; & compared with Low-SHK group, $P \leq 0.05$; △ compared with Middle-SHK group, $P \leq 0.05$.

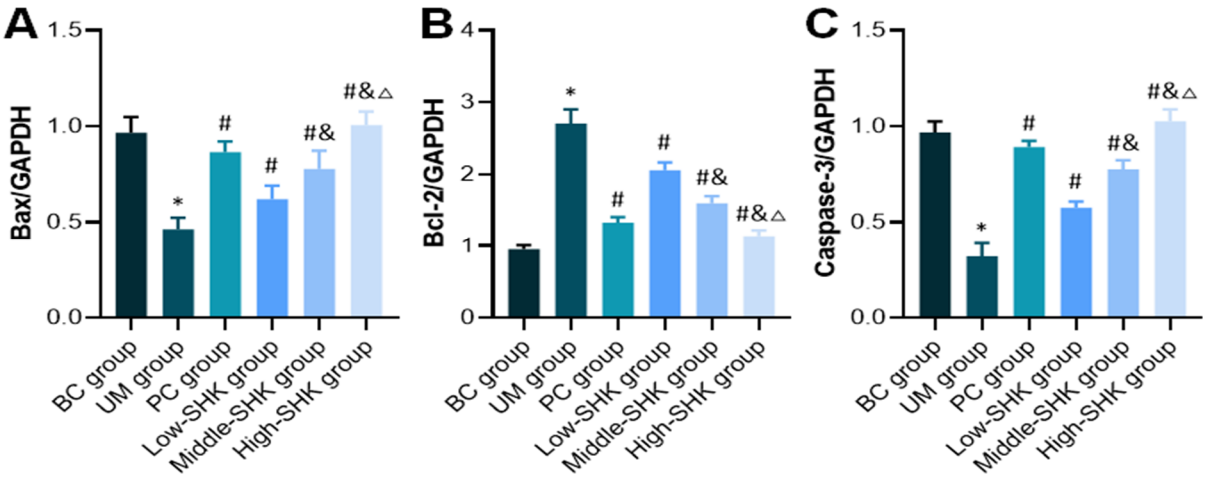

Fig. 4 Comparison of distinctions in the relative expression of apoptosis-related mRNA in the uterus of mice. A: relative expression of Bax; B: relative expression of Bcl-2; C: relative expression of Cas-3. * Compared with BC group, $P \leq 0.05$; # compared with UM group, $P \leq 0.05$; & compared with Low-SHK group, $P \leq 0.05$; △ compared with Middle-SHK group, $P \leq 0.05$.

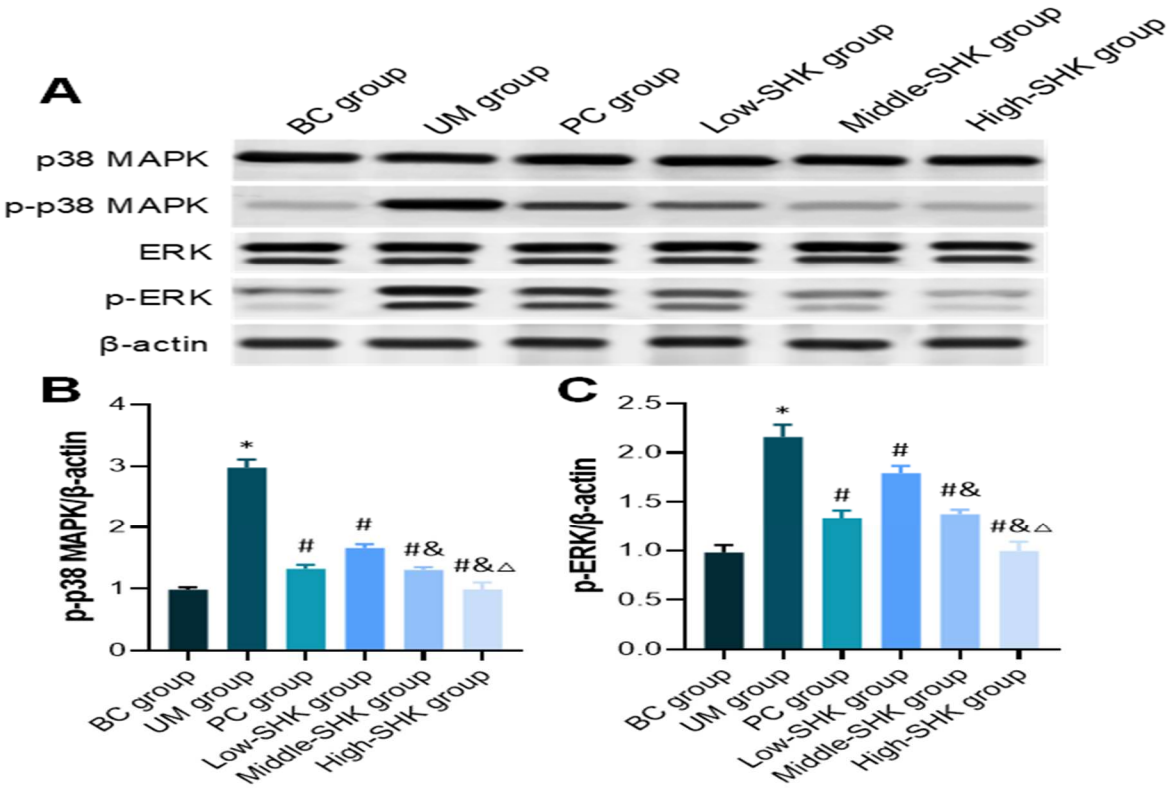

Fig. 5 Comparison of distinctions in the relative expression of proteins related to the MAPK/ERK pathway in the uterus of mice. A: Western blotting; B: relative expression of p-p38 MAPK; C: relative expression of p-ERK. * Compared with BC group, $P \leq 0.05$; # compared with UM group, $P \leq 0.05$; & compared with Low-SHK group, $P \leq 0.05$; △ compared with Middle-SHK group, $P \leq 0.05$.

were markedly higher, while the level of AMH (Figure 3G) was markedly lower in the UM group relative to BC group; the levels of peripheral blood serum estradiol, progesterone, luteinizing hormone, estrogen receptor, progesterone receptor, and follicle-stimulating hormone were markedly lower, while the level of AMH was markedly higher in PC group, Low-SHK group, Middle-SHK group, and High-SHK group relative to UM group;

with the increase of SHK dosage, the levels of peripheral blood serum estradiol, progesterone, luteinizing hormone, estrogen receptor, progesterone receptor, and follicle-stimulating hormone gradually decreased, and the level of AMH gradually increased in Low-SHK group, Middle-SHK group and High-SHK group ($P \leq 0.05$).

Effects of SHK on the expression of Bax, Bcl-2, and Cas-3 mRNA in the uterus of UM mice: In Figure 4A to 4C, the relative expression of Bax and Cas-3 mRNA were markedly lower, while the relative expression of Bcl-2 mRNA was markedly higher in the uterus of UM group relative to BC group; the relative expression of Bax and Cas-3 mRNA were markedly higher, while the relative expression of Bcl-2 mRNA was markedly lower in the uterus of PC group, Low-SHK group, Middle-SHK group and High-SHK group relative to UM group; with the increase of SHK dosage, the relative expression of Bax and Cas-3 mRNA gradually increased, while the relative expression of Bcl-2 mRNA gradually decreased in the uterus of Low-SHK group, Middle-SHK group and High-SHK group ($P \leq 0.05$).

Effects of the expression of proteins related to the MAPK/ERK pathway: In Figure 5A to 5C, no visible distinction was noted in the relative expression of p38 MAPK and ERK in the uterus of the six groups ($P > 0.05$). The relative expression of p-p38 MAPK and p-ERK in the uterus of the UM group was markedly higher in contrast to BC group; the relative expression in PC group, Low-SHK group, Middle-SHK group, and High-SHK group was markedly lower in contrast to UM group; with the increase of SHK dosage, the relative expression in Low-SHK group, Middle-SHK group, and High-SHK group gradually decreased ($P \leq 0.05$).

DISCUSSION

In this work, the UM mouse model was prepared by continuous intramuscular injection of estradiol benzoate + Tween80 + 0.9% sodium chloride for 15 d, and it was found that compared with normal mice, the uterine tumors, vertical diameter, horizontal diameter, uterine coefficient, and smooth muscle thickness of the UM mice all increased markedly. It was also found that after treatment with different doses of SHK, the uterine tumors, vertical diameter, horizontal diameter, uterine coefficient, and smooth muscle thickness of the UM mice all decreased markedly, and the phosphorylation levels of p38 MAPK and ERK in the uterine tissue decreased, showing a dose-dependent characteristic. UM is common in women of childbearing age, and their incidence increases with age. It is the hormone-dependent tumor, and sex hormones can promote the development of UM (Vannuccini *et al*., 2024). At present, the induction of UM animal models by estradiol benzoate has been widely adopted (Yousefi *et al*., 2021; Mamoon *et al*., 2021). Further findings showed that in the uterine tissue of the UM mouse model induced by estradiol benzoate, smooth muscle cells showed focal necrosis or hyperplasia, accompanied by pathological manifestations of inflammatory cell infiltration. This indicates that UM is related to the abnormal proliferation and apoptosis of USM cells. However, the pathogenesis of UM is complex, involving changes in sex hormones and their receptors, local peptide growth factors, etc., among which ovarian hormone dependence has become a consensus (Awiwi *et al*., 2022). Both estrogen and progesterone can stimulate the progression of UM disease, and various hormones and their receptors in the body combine to exert biological effects (Zhao *et al*., 2022). It was found that in the peripheral blood of the UM mouse model, the levels of serum estradiol, progesterone, luteinizing hormone, estrogen receptor, progesterone receptor, and follicle-stimulating hormone increased, and the level of AMH decreased. It aligns with the findings of Liang *et al*. (2024). This indicates that the progression of UM is closely related to the changes in the levels of sex hormones in the body (Liang *et al*., 2024).

SHK is the main active ingredient in Lithospermum, and it has biological activities such as anti-inflammatory, antibacterial, and anti-tumor effects (Kaur *et al*., 2022). Current research has confirmed that SHK has anti-tumor activity against multiple types of tumors. Tang *et al*. (2020) found that SHK can suppress the survival, migration, and invasion of cervical cancer Hela and C33a cells in a dose-dependent manner, and induce cell cycle arrest and epithelial-mesenchymal transition, thereby exerting anti-cervical cancer effects (Tang *et al*., 2020). Han *et al*. (2018) developed the anti-tumor activity of the SHK derivative PMMB232 and found that it can bind to HIF-1α to inhibit the proliferation of cervical cancer Hela cells, mainly by affecting the expression of proteins such as E-cadherin to exert anti-tumor effects (Han *et al*., 2018). To understand the potential action of the anti-UM activity of SHK, the effects of SHK on the serum sex hormone levels of UM mice were analyzed. Serum estradiol can increase the vitality of uterine arteries, and the local increase of serum estradiol in UM can induce an increase in the activity of nitric oxide synthase, thereby promoting uterine vasodilation, improving the blood supply of UM, and ultimately promoting tumor growth (Ali *et al.*, 2022; Al-Hendy *et al*., 2021). Abnormal proliferation of UM cells can enhance the activation degree of estrogen receptor and progesterone receptor, which further promotes the proliferation of fibroid cells (Beck *et al*., 2022). Luteinizing hormone and follicle-stimulating hormone can act in synergy with prolactin to stimulate the growth of UM (Wrona *et al*., 2022). In addition, ovarian function also depends on changes in sex hormone levels, especially serum estradiol, follicle-stimulating hormone, and AMH. When ovarian reserve function declines, the

negative feedback of inhibin B released by pituitary follicles on the pituitary decreases, resulting in an increase in follicle-stimulating hormone levels (Tang and Li, 2022). AMH is released from antral follicles, and a decrease in its level is a sign of impaired ovarian reserve function (Mollhuijsen *et al*., 2020). It was found that after treatment with different doses of SHK, serum estradiol, progesterone, luteinizing hormone, estrogen receptor, progesterone receptor, and follicle-stimulating hormone in the peripheral blood of UM mice decreased, while AMH increased, showing a dose-dependent characteristic. This indicates that SHK can suppress the growth of UM and improve ovarian reserve function by affecting the changes in sex hormone levels in the body.

Abnormal apoptosis programs can lead to disordered apoptosis of USM cells, hinder the normal clearance and renewal process of abnormal cells, and inhibit the apoptosis of USM cells (Szydłowska *et al*., 2021; Tunau *et al*., 2021; Zhao *et al*., 2022). After Bax is activated, it can be transferred to the mitochondrial membrane and interact with Pore protein on the membrane to enhance its permeability, thereby promoting the release of cytochrome C and activating Cas-3 or Caspase-9, which induce apoptosis (Hu *et al*., 2020). Bcl-2 can prevent the release of cytochrome C from mitochondria and block the initiation of the apoptotic cascade (Joung *et al*., 2022). It was found that in the uterine tissue of UM mice, the relative expression of Bax and Cas-3 mRNA had a decrease, while the relative expression of Bcl-2 mRNA had a raise. This suggests that in UM tissue, the pro-apoptotic genes Bax and Cas-3 are lowly expressed or down-regulated, while the anti-apoptotic gene Bcl-2 is highly expressed or up-regulated. It was also found that after treatment with different doses of SHK, the relative expression of Bax and Cas-3 mRNA in the uterine tissue of UM mice increased, while the relative expression of Bcl-2 mRNA decreased, showing a dose-dependent characteristic. This is similar to the results found by Qi *et al*. (2022) that SHK can down-regulate Bcl-2 and activate Cas-3/9 to induce apoptosis of colorectal cancer cells (Qi *et al*., 2022). It indicates that SHK can promote the apoptosis of USM cells in UM, thereby exerting an anti-tumor growth effect.

Serum estradiol, when combined with estrogen receptor, can promote the proliferation of USM cells by activating pathways, thereby promoting tumor growth (Ishikawa *et al*., 2024). The MAPK/ERK pathway plays a major role in UM (Reschke *et al*., 2022). The MAPKs cascade system is one of the highly conserved pathways in eukaryotic cells. Under the stimulation of cytokines, etc., the p38 MAPK and ERK1/2 pathways are activated. The MAPK cascade gradually activates downstream target molecules, which further affect the participation of multiple downstream cytokines in immune responses or inflammatory reactions (Ding *et al*., 2023; Wang *et al*., 2024). It was found that in the uterine tissue of UM mice, the phosphorylation levels of p38 MAPK and ERK increased, while different doses of SHK could markedly inhibit the phosphorylation, showing a dose-dependent characteristic. The MAPK/ERK pathway in UM is abnormally activated and can become a potential target for the treatment of UM. Shan *et al*. (2017) found that SHK can suppress the activation of the ERK pathway in periodontal ligament cells and promote the phosphorylation of p38 in leukemia NB4 cells to induce apoptosis (Shan *et al*., 2017). The specific application and effect of suppressing the activation of the MAPK/ERK pathway in the treatment of UM still need further research and verification. Compared to commonly used clinical drugs (such as GnRH analogs or selective progesterone receptor modulators), SHK demonstrates similar efficacy in improving uterine morphology and sex hormone imbalances but may carry a lower risk of endocrine disruption (Beck *et al.,* 2022). Although GnRH analogs can reduce fibroid size, their long-term use is associated with a risk of osteoporosis, whereas SHK, through multi-target regulation, may reduce such side effects. This study confirmed that SHK markedly improves UM pathological changes by inhibiting the phosphorylation of the MAPK/ERK pathway (p-p38 MAPK, p-ERK). However, as a multi-target natural product, SHK may also regulate other signaling pathways. Previous study has reported that SHK inhibits the proliferation of cervical cancer cells via FAK/AKT/GSK3β signalling (Xu *et al.,* 2022). Although these pathways were not examined in this study, the possibility of SHK inhibiting UM through multi-pathway synergistic effects can't be ruled out. Previous studies on SHK focused primarily on cancers such as cervical or colorectal tumors, with limited exploration of its efficacy in benign hormone-dependent tumors like UM. Our findings fill this gap by demonstrating SHK's dual role in restoring hormonal balance and suppressing MAPK/ERK activation in UM.

Limitations of this study include the failure to assess other potential pathways (such as Wnt/β-catenin) and the relatively short experimental duration, lacking long-term efficacy data. Future research should incorporate transcriptomics and long-term toxicity studies to further validate the findings. Comprehensive analysis through whole-genome or proteomics studies would allow for a systematic evaluation of SHK's off-target effects and its global regulatory mechanisms in UM.

Conclusion: SHK can suppress the abnormal activation of the MAPK/ERK pathway in a dose-dependent manner, thereby regulating the abnormal changes in sex hormone levels in UM mice and promoting the apoptosis of USM cells to improve the pathological tissue changes in the uterus. This work can offer a help to explore the specific role and mechanism of the MAPK/ERK pathway in UM, and is significant for the development of new treatment

methods and the improvement of therapeutic effects for UM.

Authors' Contributions: Jianhua Wang designed experiments; Jianhua Wang analyzed data; Jianhua Wang collected samples; Jianhua Wang performed experiments; Jianhua Wang wrote and revise the manuscript. The author agreed to publish this article.

Animal rights statement: All animal experiments were approved by the Animal Ethics Committee of The Fourth Hospital of Changsha (Changsha, China), in compliance with Chinese national guidelines for the care and use of animals.

REFERENCES

Afrin, S., M. Ramaiyer, U.A.M. Begum and M.A. Borahay (2023). Adipocyte and Adipokines Promote a Uterine Leiomyoma Friendly Microenvironment. Nutrients. 15(3):715. https://doi.org/10.3390/nu15030715

Awiwi, M.O., M. Badawy, A.M. Shaaban, C.O. Menias, J.M. Horowitz, M. Soliman, C.T. Jensen, A.H. Gaballah, J.J. Ibarra-Rovira, M.K. Feldman, M.X. Wang, P.S. Liu and K.M. Elsayes (2022). Review of uterine fibroids: imaging of typical and atypical features, variants, and mimics with emphasis on workup and FIGO classification. Abdom Radiol (NY). 47(7):2468–2485. https://doi.org/10.1007/s00261-022-03545-x

Ahmad, A., M. Kumar, N.R. Bhoi, Badruddeen, J. Akhtar, M.I. Khan, M. Ajmal and M. Ahmad (2023). Diagnosis and management of uterine fibroids: current trends and future strategies. J Basic Clin Physiol Pharmacol. 34(3):291–310. https://doi.org/10.1515/jbcpp-2022-0219

Al-Hendy, A., A.S. Lukes, A.N. 3rd Poindexter, R. Venturella, C. Villarroel, H.O.D. Critchley, Y. Li, L. McKain, J.C. Arjona Ferreira, A.G.M. Langenberg, R.B. Wagman and E.A. Stewart (2021). Treatment of Uterine Fibroid Symptoms with Relugolix Combination Therapy. N Engl J Med. 384(7):630–642. https://doi.org/10.1056/NEJMoa2008283

Ali, M., H.Y. Chen, Y.F. Chiang, O.A. Badary, S.M. Hsia and A. Al-Hendy (2022). An evaluation of relugolix/estradiol/norethindrone acetate for the treatment of heavy menstrual bleeding associated with uterine fibroids in premenopausal women. Expert Opin Pharmacother. 23(4):421-429. https://doi.org/10.1080/14656566.2022.2030705

Barkizatova, G., A. Turgumbayeva, K. Zhakipbekov, K. Bekesheva, Z. Arystanov, T. Arystanova, F. Kayupova, K. Zhumalina, Z. Toxanbayeva, A. Ibragimova, O. Blinova, G. Utegenova, N. Iztileu and Z. Shynykul (2024). Exploring the Pharmacological Potential of Lithospermum officinale L.: A Review of Phytochemicals and Ethnomedicinal Uses. Molecules. 29(8):1856. https://doi.org/10.3390/molecules29081856

Beck, D., I. Winzenborg, M. Liu, J. Degner, N.M. Mostafa, P. Noertersheuser and M. Shebley (2022). Population Pharmacokinetics of Elagolix in Combination with Low-Dose Estradiol/Norethindrone Acetate in Women with Uterine Fibroids. Clin Pharmacokinet. 61(4):577–587. https://doi.org/10.1007/s40262-021-01096-w

Donnez, J., H.S. Taylor, L. Marcellin and M.M. Dolmans (2024). Uterine fibroid-related infertility: mechanisms and management. Fertil Steril. 122(1):31–39. https://doi.org/10.1016/j.fertnstert.2024.02.049

Ding, A.J., W.M. Zhang, J. Tao, B. Chen, X.C. Liu, Y. Dong, H.J. Ma, S.D. Pan, J.B. He and W.K. Zeng (2023). *Salmonella enterica* serovar Paratyphi A-induced immune response in *Caenorhabditis elegans* depends on MAPK pathways and DAF-16. Front Immunol. 14:1118003. https://doi.org/10.3389/fimmu.2023.1118003

Fasciani, A., G. Turtulici, A. Pedullà and R. Sirito (2023). Uterine Myoma Position-based Radiofrequency Ablation (UMP-b RFA): 36 months follow-up clinical outcomes. Eur J Obstet Gynecol Reprod Biol. 281:23–28. https://doi.org/10.1016/j.ejogrb.2022.12.006

Han, H.W., C.S. Zheng, S.J. Chu, W.X. Sun, L.J. Han, R.W. Yang, J.L. Qi, G.H. Lu, X.M. Wang and Y.H. Yang (2018). The evaluation of potent antitumor activities of shikonin coumarin-carboxylic acid, PMMB232 through HIF-1α-mediated apoptosis. Biomed Pharmacother. 97:656–666. https://doi.org/10.1016/j.biopha.2017.10.159

Hu, L., M. Chen, X. Chen, C. Zhao, Z. Fang, H. Wang and H. Dai (2020). Chemotherapy-induced pyroptosis is mediated by BAK/BAX-caspase-3-GSDME pathway and inhibited by 2-bromopalmitate. Cell Death Dis. 11(4):281. https://doi.org/10.1038/s41419-020-2476-2

Ishikawa, H., Y. Goto, C. Hirooka, E. Katayama, N. Baba, M. Kaneko, Y. Saito, T. Kobayashi and K. Koga (2024). Role of inflammation and immune response in the pathogenesis of uterine fibroids: Including their negative impact on reproductive outcomes. J Reprod Immunol. 165:104317. https://doi.org/10.1016/j.jri.2024.104317

Joung, J., P.C. Kirchgatterer, A. Singh, J.H. Cho, S.P. Nety, R.C. Larson, R.K. Macrae, R. Deasy, Y.Y. Tseng, M.V. Maus and F. Zhang (2022). CRISPR activation screen identifies BCL-2 proteins and B3GNT2 as drivers of cancer resistance to T cell-mediated cytotoxicity. Nat Commun. 13(1):1606. https://doi.org/10.1038/s41467-022-29205-8

Kaur, K., R. Sharma, A. Singh, S. Attri, S. Arora, S. Kaur and N. Bedi (2022). Pharmacological and analytical aspects of alkannin/shikonin and their derivatives: An update from 2008 to 2022. Chin Herb Med. 14(4): 511–527. https://doi.org/10.1016/j.chmed.2022.08.001

Lee, S. and E.A. Stewart (2023). New treatment options for nonsurgical management of uterine fibroids. Curr Opin Obstet Gynecol. 35(4):288–293. https://doi.org/10.1097/GCO.0000000000000880

Liang, Y., R. Yang, Y. Wei, B. Huang, Y. Chen, X. Zhang, J. Yao, G. Wang, H. Mao, H. Shi, Q. Yang, J. Tang, M. Ji, K. Hua and S. Yao (2024). Multicenter, prospective, single-arm clinical study to investigate the efficacy and safety of Zoladex (Goserelin acetate) 10.8 mg prior to surgery in Chinese premenopausal women with symptomatic uterine fibroids. Gynecol Endocrinol. 40(1):2427190. https://doi.org/10.1080/09513590.2024.2427190

Liu, Q., X. Chen, Y. Tan, J. Liu, M. Zhu, D. Li, Y. Zhou, T. Zhang and Q.Z. Yin (2024). Natural products as glycolytic inhibitors for cervical cancer treatment: A comprehensive review. Biomed Pharmacother. 175:116708. https://doi.org/10.1016/j.biopha.2024.116708

Long, L., W. Xiong, F. Lin, J. Hou, G. Chen, T. Peng, Y. He, R. Wang, Q. Xu and Y. Huang (2023). Regulating lactate-related immunometabolism and EMT reversal for colorectal cancer liver metastases using shikonin targeted delivery. J Exp Clin Cancer Res. 42(1):117. https://doi.org/10.1186/s13046-023-02688-z

Mamoon, R.S., A.S. Mawas, S.M. El Badry, A.M. Youssef, M.G. Ali, M.A. Aly and A.M. Abo El-Maaty (2021). Therapeutic modality of induced uterine leiomyoma with shock waves in rats: The uterine blood flow, circulating ovarian hormones and histopathological findings. Reprod Biol. 21(2):100501. https://doi.org/10.1016/j.repbio.2021.100501

Moolhuijsen, L.M.E. and J.A. Visser (2020). Anti-Müllerian Hormone and Ovarian Reserve: Update on Assessing Ovarian Function. J Clin Endocrinol Metab.105(11):3361–3373. https://doi.org/10.1210/clinem/dgaa513

Ni, M., J. Zhou, Z. Zhu, Q. Xu, Z. Yin, Y. Wang, Z. Zheng and H. Zhao (2023). Shikonin and cisplatin synergistically overcome cisplatin resistance of ovarian cancer by inducing ferroptosis via upregulation of HMOX1 to promote Fe2+ accumulation. Phytomedicine. 112:154701. https://doi.org/10.1016/j.phymed.2023.154701

Qian, X., L. Zhu, M. Xu, H. Liu, X. Yu, Q. Shao and J. Qin (2023). Shikonin suppresses small cell lung cancer growth via inducing ATF3-mediated ferroptosis to promote ROS accumulation. Chem Biol Interact. 382:110588. https://doi.org/10.1016/j.cbi.2023.110588

Qi, H., X. Zhang, H. Liu, M. Han, X. Tang, S. Qu, X. Wang and Y. Yang (2022). Shikonin induced Apoptosis Mediated by Endoplasmic Reticulum Stress in Colorectal Cancer Cells. J Cancer. 13(1):243–252. https://doi.org/10.7150/jca.65297

Reschke, L., S. Afrin, M. El Sabah, N. Charewycz, M. Miyashita-Ishiwata and M.A. Borahay (2022). Leptin induces leiomyoma cell proliferation and extracellular matrix deposition via JAK2/STAT3 and MAPK/ERK pathways. F S Sci. 3(4):383–391. https://doi.org/10.1016/j.xfss.2022.05.001

Shafiee, M., N. S. Aghili Moghaddam, M. Nosrati, M. Tousi, A. Avan, M. Ryzhikov, M. R. Parizadeh, H. Fiuji, M. Rajabian, A. Bahreyni, M. Khazaei and S. M. Hassanian (2017). Saffron against Components of Metabolic Syndrome: Current Status and Prospective. J Agric Food Chem. 65(50):10837-10843. https://doi.org/10.1021/acs.jafc.7b03762.

Shan, Z.L., L. Zhong, C.L. Xiao, L.G. Gan, T. Xu, H. Song, R. Yang, L. Li and B.Z. Liu (2017). Shikonin suppresses proliferation and induces apoptosis in human leukemia NB4 cells through modulation of MAPKs and c-Myc. Mol Med Rep. 16(3):3055–3060. https://doi.org/10.3892/mmr.2017.6965

Sun, Q., T. Gong, M. Liu, S. Ren, H. Yang, S. Zeng, H. Zhao, L. Chen, T. Ming, X. Meng and H. Xu (2022). Shikonin, a naphthalene ingredient: Therapeutic actions, pharmacokinetics, toxicology, clinical trials and pharmaceutical researches. Phytomedicine. 94:153805. https://doi.org/10.1016/j.phymed.2021.153805

Szydłowska, I., M. Grabowska, J. Nawrocka-Rutkowska, M. Piasecka and A. Starczewski (2021). Markers of Cellular Proliferation, Apoptosis, Estrogen/Progesterone Receptor Expression and Fibrosis in Selective Progesterone Receptor Modulator (Ulipristal Acetate)-Treated Uterine Fibroids. J Clin Med. 10(4):562. https://doi.org/10.3390/jcm10040562

Tang, Q., L. Liu, H. Zhang, J. Xiao and S.S. Hann (2020). Regulations of miR-183-5p and Snail-Mediated Shikonin-Reduced Epithelial-Mesenchymal Transition in Cervical Cancer Cells. Drug Des Devel Ther. 14:577–589. https://doi.org/10.2147/DDDT.S236216

Tang, Y and Y. Li (2022). Evaluation of Serum AMH, INHB Combined with Basic FSH on Ovarian Reserve Function after Laparoscopic Ovarian Endometriosis Cystectomy. Front Surg. 9:906020. https://doi.org/10.3389/fsurg.2022.906020

Tunau, K.A., J.A. Garba, A.A. Panti, C.E. Shehu, A.N. Adamu, M.B. AbdulRahman and M.K. Ahmad (2021). Low plasma vitamin D as a predictor of uterine fibroids in a nigerian population. Niger Postgrad Med J. 28(3):181–186. https://doi.org/10.4103/npmj.npmj_495_21

Vannuccini, S., F. Petraglia, F. Carmona, J. Calaf and C. Chapron (2024). The modern management of uterine fibroids-related abnormal uterine bleeding. Fertil Steril. 122(1):20-30. https://doi.org/10.1016/j.fertnstert.2024.04.041

Wang, Q., J.Y. Zhou, L. Liu, Z.Y. Yin, Y.Y. Li, M. Wang, J.B. Zhang, H. Lu, X.Y. Zhou and B. Zhang (2024). Resveratrol activates MAPK/ERK pathway to regulate oestrogen metabolism in type I endometrial cancer. BMC Complement Med Ther. 24(1):227. https://doi.org/10.1186/s12906-024-04509-y

Wrona, A., V. Aleksandrovych, T. Bereza, P. Basta, A. Gil, M. Ulatowska-Białas, M. Mazur-Laskowska, K. Pityński and K. Gil (2022). Oviductal Oxygen Homeostasis in Patients with Uterine Myoma: Correlation between Hypoxia and Telocytes. Int J Mol Sci. 23(11):6155. https://doi.org/10.3390/ijms23116155

Xu, Z., L. Huang, T. Zhang, Y. Liu, F. Fang, X. Wu, W. Chen, L. Lan, Y. Zhang, N. Li and P. Hu (2022). Shikonin inhibits the proliferation of cervical cancer cells via FAK/AKT/GSK3β signalling. Oncol Lett. 24(3):304. https://doi.org/10.3892/ol.2022.13424

Yadav, S., A. Sharma, G.A. Nayik, R. Cooper, G. Bhardwaj, H.S. Sohal, V. Mutreja, R. Kaur, F.O. Areche, M. AlOudat, A.M. Shaikh, B. Kovács and A.E. Mohamed Ahmed (2022). Review of Shikonin and Derivatives: Isolation, Chemistry, Biosynthesis, Pharmacology and Toxicology. Front Pharmacol. 13:905755. https://doi.org/10.3389/fphar.2022.905755

Yan, C., Q. Li, Q. Sun, L. Yang, X. Liu, Y. Zhao, M. Shi, X. Li and K. Luo (2023). Promising Nanomedicines of Shikonin for Cancer Therapy. Int J Nanomedicine. 18:1195–1218. https://doi.org/10.2147/IJN.S401570

Yousefi, B., V. Semnani, T. Mokhtari, S. Zarbakhsh, M.H.T. Amjad, M. Barati and H. Doustmohammadi (2021). Co-administration of Aluminum Sulfate and Propolis Regulates Matrix Metalloproteinases-2/9 Expression and Improves the Uterine Leiomyoma in Adult Rat Model. Biol Trace Elem Res. 199(3):1002–1012. https://doi.org/10.1007/s12011-020-02200-0

Zhao, C., S.T. Lu, Y. Wang, P. Hu, L. Yan, M.B. Liu, L.B. Liu and L. Lei (2022). Hysteroscopic management of a “hernia-like” uterine myoma within the uterine cavity. Fertil Steril. 118(6):1199–1200. https://doi.org/10.1016/j.fertnstert.2022.08.857

Zhao, W., Y. Zhao, L. Chen, Y. Sun and S. Fan (2022). Effects of miRNA-199a-5p on cell proliferation and apoptosis of uterine leiomyoma by targeting MED12. Open Med (Wars). 17(1):151–159. https://doi.org/10.1515/med-2021-0348.